Effects of curvature on triple flame propagation in fuel-oxidizer counterflow

Shumeng Xie[1], Dehai Yu[1], Joel Daou[2], Zheng Chen[1*]

[1]SKLTCS, CAPT, College of Engineering, Peking University, Beijing, 100871, China

[2]Department of Mathematics, University of Manchester, Manchester, UK

Abstract

In this study, we analyze the propagation of an expanding triple flame in an axisymmetric counterflow of a fuel against an oxidizer. The problem is formulated as a thermo-diffusive model with one-step global reaction. An asymptotic analysis in the limit of large activation energy and weak strain rate is conducted. The study is supported and complemented by numerical simulations carried out for arbitrary values of the strain rate. In addition to the flame front curvature $1/R_t$ associated with the variation in the reactants concentrations transverse to the mixing layer, the propagation of the expanding triple flame also depends on the azimuthal curvature $1/R_f$ where R_f is the front leading edge radial distance. As the triple flame expands to large radial distances, its propagation becomes quasi-steady. Under a quasi-steady state assumption, an explicit expression is derived for the displacement speed of the triple flame, which is found to be linearly proportional to the total curvature $1/R_f + 1/R_t$. Two-dimensional axisymmetric simulations are conducted to validate in particular the quasi-steady assumption. These include transient simulations of the expanding triple flame which are compared to the numerical solution of the steady eigenvalue problem obtained in a frame attached to the propagating front under a quasi-steady assumption. Following a transient ignition phase, the triple flame is found to propagate in a quasi-steady manner when R_f (measured with the stoichiometric planar flame thickness) exceeds 5, approximately. Although the theoretical analysis is performed in the weak strain limit, the linear dependence of the triple flame speed on the curvature $1/R_f$ is found to be applicable over a wide range of strain rates. Besides, the analysis is extended for inwardly propagating triple flames (flame holes) and similar expressions describing the relationship between displacement speed of the triple flame and curvatures are obtained.

Keywords: Triple flame, curvature effects, axisymmetric counterflow, propagation speed

* Corresponding author. E-mail: cz@pku.edu.cn.

1. Introduction

Non-premixed combustion occurs in most engines, such as gas turbine engines and direct injection engines [1]. During the combustion in these engines, unsteady local extinction and re-ignition phenomena arise at certain locations depending on the local thermal conditions, mixture composition and flow parameters. Triple flame fronts are often observed as the separating boundary between the unburnt and burnt mixtures [2]. A triple flame may propagate or remain stationary, and is closely related to the flame flashback or blow-off in real combustors [3,4]. Given its critical role, a better comprehension of triple flame dynamics may lead to improved engine design. This study will assess the curvature effects on triple flame propagation speed.

The triple flame propagation speed is larger than laminar flame speed of the corresponding stoichiometric mixture by a factor that scales with the square root of the fresh-to-burnt density ratio. The thermal expansion across the flame sheet and the flow redirection ahead the flame front were found to be responsible for the acceleration of triple flame [5]. Various regimes of triple flame were identified through extensive theoretical [6–12], numerical [3,13–17] and experimental [3,18–23] studies. Grib and Renfro [14] summarized the recent progress on triple flames and provided a descriptive triple/edge flame map based on an energy budget analysis.

It is well known that the triple flame strongly depends on the local concentration gradient or mixing layer thickness. Daou and coworkers [7–10] have systematically analyzed the triple flame propagation in a planar counterflow, in which the mixing layer thickness is inversely proportional to the square root of strain rate. They derived an explicit formula for triple flame speed using large activation energy asymptotic analyses, and assessed the influence of various factors including preferential diffusion, heat loss and the reversibility of the chemical reaction. The correlations derived in theoretical analyses were verified by computational [3,14] and experimental studies [3,21–23].

In turbulent combustion, the triple flame is always stretched and multi-dimensional, and it is subjected to spatially varying concentration gradients [2]. Therefore, there could exist another part of curvature, which is absent in planar counterflow or co-flow jet configuration [3,7–10,21]. A sketch of an expanding triple flame in the axisymmetric counterflow configuration is depicted in Fig. 1. The triple flame is initiated by a hot spot or spark at the stagnation point, and it can propagate outwardly in a self-sustained manner if the ignition energy is above some critical value [24]. Figure 1 shows that the curvature of the expanding triple flame consists of two parts: the azimuthal curvature, $1/R_f$, which is the inverse of the radial distance from the triple point to the origin and which decreases during the triple flame propagation; and the curvature, $1/R_t$, which is associated with the variation in the reactants concentrations transverse to the mixing layer and is therefore determined by the mixing layer thickness and thereby the stain rate of the counterflow.

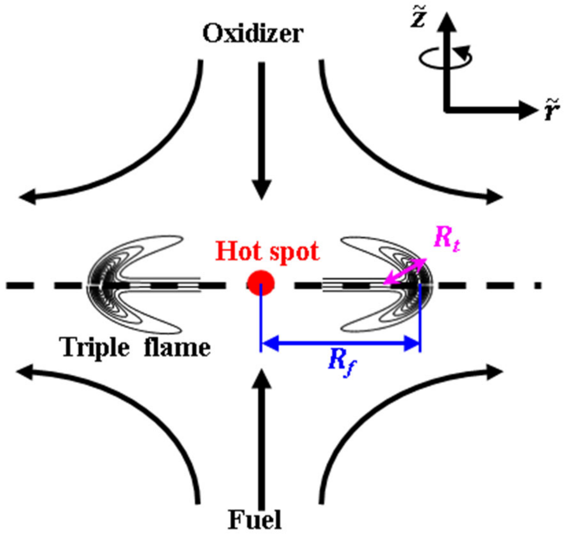

Fig. 1 Schematic of the expanding triple flame initiated by a hot spot or spark at the stagnation point of the counterflow of fuel against oxidizer. The radius R_f refers to the distance from the triple flame to the axis of symmetry, and the radius R_t depends on the stain rate of the counterflow.

The effects of the curvature $1/R_t$ determined by the mixing layer thickness on triple flame propagation has been thoroughly discussed in the literature [3,7,9]. However, the effects of azimuthal curvature $1/R_f$ received little attention, which motivates the present work. Therefore, the objective of this study is to assess the effects of the curvature $1/R_f$ on the propagation speed of the expanding triple flame in a counterflow configuration. An asymptotic analysis in the limit of large activation energy and weak strain rate is conducted for the expanding triple flame, within a thermo-diffusive model with one-step global reaction. An explicit expression is derived for the displacement speed of the expanding triple flame, which quantifies the effects of both curvatures on triple flame propagation.

The paper is structured as follows. In Section 2, a model for the expanding triple flame in an axisymmetric counterflow is formulated. Section 3 presents a detailed asymptotic analysis and its theoretical results. To validate the theoretical analysis, two-dimensional simulations are conducted and the results are presented in Section 4. In addition to the expanding triple flame disc, the inwardly propagating flame hole with negative azimuthal curvature is also considered in Section 5 in order to extend the range of applicability of analytical results. Finally, the conclusions are summarized in Section 6.

2. Model and formulation

We consider an expanding triple flame in a two-dimensional axisymmetric counterflow configuration as shown in Fig. 1. A cylindrical coordinate system has its origin located at the stagnation point of the counterflow. Oxidizer and fuel streams are injected against each other from $\tilde{z} = \pm\infty$, resulting in a mixing layer around the stagnation surface at $\tilde{z} = 0$. A hot spot at the stagnation point is used to ignite the triple flame [24]. Successful ignition results in an expanding triple flame propagating along the radial direction. The present model differs from that used by Daou and coworkers [7–9], in which the counterflow is planar and hence no azimuthal curvature affecting triple flame propagation is present.

For mathematical simplicity, we adopt a thermal-diffusive model with constant density (denoted as ρ), which decouples the flow with combustion process due to the absence of thermal expansion. The ideal potential flow characterized by the strain rate a is prescribed. The flow field is hence given as $\tilde{u}_{\tilde{r}} = a\tilde{r}$ and $\tilde{u}_{\tilde{z}} = -2a\tilde{z}$. We consider the one-step irreversible reaction with the fuel consumption rate following the Arrhenius law, $\tilde{\omega}_F = B\rho^2 Y_F Y_O \exp(-E_a/R_0 T)$, in which B is the pre-exponent factor, E_a the activation energy, R_0 the universal constant, Y_F and Y_O the mass fraction of fuel and oxidizer, and T the temperature. The following non-dimensional variables are introduced

$$t = \frac{\tilde{t}S_L^0}{\delta_f}, \qquad r = \frac{\tilde{r}}{\delta_f}, \qquad z = \frac{\tilde{z}}{\delta_f}, \qquad \theta = \frac{T - T_u}{T_b - T_u}, \qquad y_F = \frac{Y_F}{Y_{F,st}}, \qquad y_O = \frac{Y_O}{Y_{O,st}}, \tag{1}$$

in which S_L^0 is the laminar flame speed of a stoichiometric mixture, $\delta_f = D_T/S_L^0$ the flame thickness of the corresponding premixed planar flame (in which D_T is the thermal diffusivity), T_u the unburnt temperature of incoming flow, and T_b the adiabatic flame temperature. Here $Y_{F,st}$ and $Y_{O,st}$ represent the stoichiometric mass fraction of the fuel and oxidizer, respectively.

For the axisymmetric counterflow with specified ideal potential flow, the non-dimensional governing equations for temperature and reactants' mass fractions are

$$\begin{cases} \dfrac{\partial \theta}{\partial t} + \lambda r \dfrac{\partial \theta}{\partial r} - 2\lambda z \dfrac{\partial \theta}{\partial z} = \dfrac{1}{r}\dfrac{\partial}{\partial r}\left(r\dfrac{\partial \theta}{\partial r}\right) + \dfrac{\partial^2 \theta}{\partial z^2} + \omega, \\ \dfrac{\partial y_F}{\partial t} + \lambda r \dfrac{\partial y_F}{\partial r} - 2\lambda z \dfrac{\partial y_F}{\partial z} = \dfrac{1}{Le_F}\left[\dfrac{1}{r}\dfrac{\partial}{\partial r}\left(r\dfrac{\partial y_F}{\partial r}\right) + \dfrac{\partial^2 y_F}{\partial z^2}\right] - \omega, \\ \dfrac{\partial y_O}{\partial t} + \lambda r \dfrac{\partial y_O}{\partial r} - 2\lambda z \dfrac{\partial y_O}{\partial z} = \dfrac{1}{Le_O}\left[\dfrac{1}{r}\dfrac{\partial}{\partial r}\left(r\dfrac{\partial y_F}{\partial r}\right) + \dfrac{\partial^2 y_F}{\partial z^2}\right] - \omega, \end{cases} \tag{2}$$

where

$$\omega = \frac{\beta^3}{4} y_F y_O e^{-\frac{\beta(1-\theta)}{1+\alpha_h(\theta-1)}}, \tag{3}$$

is the non-dimensional consumption rate, with $\beta = E(T_b - T_u)/RT_b^2$ being the Zel'dovich number, and $\alpha_h = (T_b - T_u)/T_b$ the thermal expansion coefficient. The Lewis number is defined as $Le_i = D_T/D_i$ $(i = F, O)$. The non-dimensional strain rate is $\lambda = aD_T/(S_L^0)^2$. The higher strain rate, the shorter the residence time and thereby the weaker the flame. The Damköhler number is inversely proportional to the strain rate λ.

At $r = 0$, symmetry conditions of zero gradients for θ, y_F and y_O should be satisfied. As $r \to +\infty$ the conditions correspond to the steady frozen solution given by

$$\begin{cases} \theta = 0, \\ y_F = \dfrac{1 - \mathrm{erf}\left(\sqrt{\lambda\, Le_F} z\right)}{1 - \mathrm{erf}\left(\sqrt{\lambda\, Le_F} z_{st}\right)}, \\ y_O = \dfrac{1 + \mathrm{erf}\left(\sqrt{\lambda Le_O} z\right)}{1 + \mathrm{erf}\left(\sqrt{\lambda Le_O} z_{st}\right)}, \end{cases} \tag{4}$$

where $z = z_{st}$ represents the surface of stoichiometric mixture faction, and it is determined implicitly by the following expression

$$\phi \operatorname{erf}\left(\sqrt{\lambda Le_F} z_{st}\right) + \operatorname{erf}\left(\sqrt{\lambda Le_O} z_{st}\right) = \phi - 1, \tag{5}$$

where $\phi = sY_{Fu}/Y_{Ou}$ is the global equivalence ratio for the inlet fuel and oxidizer streams and s is the mass stoichiometric ratio. The governing equations subject to the boundary conditions will be solved using an asymptotic analysis in the next section.

3. Asymptotic analysis

We aim to investigate the expanding triple flame governed by equations (2). The triple flame propagation is expected to exhibit multiple regimes corresponding to positively propagating, retreating or non-propagating flame fronts, depending on the local thermal and chemical conditions [7,25]. By means of length scale analysis, Daou and Liñán [7] considered a set of meaningful length scales, e.g. the mixing layer thickness δ_m, the local radius of the flame front R_t, the laminar flame thickness δ_f, and the thickness of preheat zone l_h, to identify the triple flame regimes for large values of the Zel'dovich number β.

Since we are concerned with the propagation of the expanding triple flame, it is convenient to choose a coordinate system attached to the moving flame front with radial position $R_f = R_f(t)$. Accordingly, we introduce the coordinate transformation

$$\tau = \varepsilon t, \qquad \xi = \varepsilon\left(r - R_f\right), \qquad \eta = \varepsilon(z - z_{st}), \tag{6}$$

in which ε is the length scale ratio defined by $\varepsilon = \delta_f/(\delta_m/\beta)$. We have $\varepsilon = \beta\sqrt{\lambda}$ since $\delta_f = D_T/S_L^0$, $\delta_m = \sqrt{D_T/a}$, and $\lambda = aD_T/(S_L^0)^2$. The leading triple flame front along the stoichiometric surface in the new transformed coordinates is illustrated in Fig. 2.

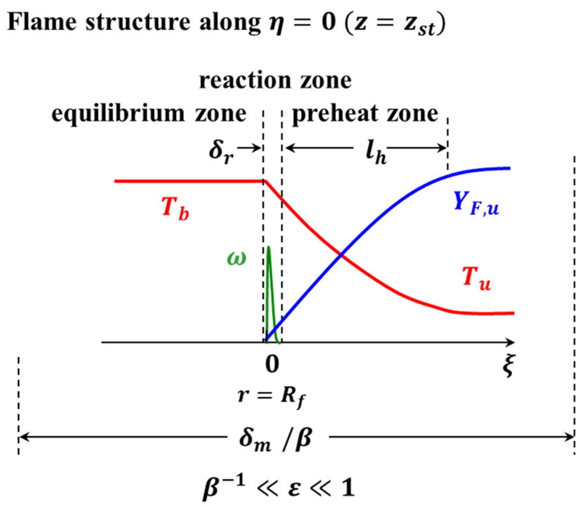

Fig. 2 Schematic of the different length scales for the expanding triple flame along the stoichiometric surface ($\eta = 0$ or $z = z_{st}$) in large activation energy limit and weak strain limit.

Here, we consider two distinguished limits, the large activation energy limit and weak strain rate limit. Relevant length scales are schematically shown in Fig. 2. Under the large activation energy limit, the chemical reaction is confined to an infinite thin layer embedded in a thin preheat zone, i.e., $\delta_r \ll l_h$. The weak strain limit is about the relative magnitude of flame thickness and mixing layer thickness, characterized by δ_r and δ_m/β. The thermal mixing layer thickness is given by $\delta_m = \sqrt{D_T/a}$, and here δ_m/β represents the characteristic flame curvature R_t within the mixing layer, as shown in Fig. 1. Under the weak strain limit, the flame front including the preheat zone is thin compared to the radius R_t depicted in Fig. 1. Consequently, the flame can be considered as quasi-planar. Following Daou and coworkers [7–9], we choose δ_m/β as the characteristic length scale. The relative magnitudes of these three length scales, δ_r, l_h and δ_m/β, are described by $\beta^{-1} \ll \varepsilon \ll 1$. This separation of length scales enables us to seek an analytical description of the triple flame structure.

In terms of the new coordinates in equation (6), the governing equations (2) become

$$\begin{cases} \frac{\partial\theta}{\partial\tau} - \left(U_f + \frac{\varepsilon}{\xi + \varepsilon R_f} - \frac{\varepsilon\xi}{\beta^2}\right)\frac{\partial\theta}{\partial\xi} - \frac{2\varepsilon(\eta + \varepsilon z_{st})}{\beta^2}\frac{\partial\theta}{\partial\eta} = \varepsilon\left(\frac{\partial^2\theta}{\partial\xi^2} + \frac{\partial^2\theta}{\partial\eta^2}\right) + \frac{\omega}{\varepsilon}, \\ \frac{\partial y_F}{\partial\tau} - \left(U_f + \frac{\varepsilon}{Le_F}\frac{1}{\xi + \varepsilon R_f} - \frac{\varepsilon\xi}{\beta^2}\right)\frac{\partial y_F}{\partial\xi} - \frac{2\varepsilon(\eta + \varepsilon z_{st})}{\beta^2}\frac{\partial y_F}{\partial\eta} = \frac{\varepsilon}{Le_F}\left(\frac{\partial^2 y_F}{\partial\xi^2} + \frac{\partial^2 y_F}{\partial\eta^2}\right) - \frac{\omega}{\varepsilon}, \\ \frac{\partial y_O}{\partial\tau} - \left(U_f + \frac{\varepsilon}{Le_O}\frac{1}{\xi + \varepsilon R_f} - \frac{\varepsilon\xi}{\beta^2}\right)\frac{\partial y_O}{\partial\xi} - \frac{2\varepsilon(\eta + \varepsilon z_{st})}{\beta^2}\frac{\partial y_O}{\partial\eta} = \frac{\varepsilon}{Le_O}\left(\frac{\partial^2 y_O}{\partial\xi^2} + \frac{\partial^2 y_O}{\partial\eta^2}\right) - \frac{\omega}{\varepsilon}, \end{cases} \quad (7)$$

where U_f is the displacement speed of the expanding triple flame. Similar to premixed flames [26], the displacement speed quantifies the propagation speed of the triple flame front relative to the local flow, and it is equal to the flame front propagation speed minus the flow speed, i.e.,

$$U_f = \frac{dR_f}{dt} - \lambda R_f = \frac{dR_f}{dt} - \frac{\varepsilon^2}{\beta^2}R_f. \quad (8)$$

It is noted that in some previous studies (e.g., [3]), the displacement speed refers to the flame front propagation speed relative to the laboratory coordinate, i.e., dR_f/dt, which is different from the one defined in this study. The definition of local triple flame speed in equation (8) is a rather simplified one and considered primarily for ease of theoretical analysis. The axial movement relative to the local flow field is neglected, which is only strictly suitable for symmetrical triple flames. Nevertheless, the triple flames in the present asymptotic analysis are almost symmetrical. The stoichiometric surface is very close to the stagnation plane. The weak strain limit assures that the local axial velocity, λz_{st}, takes a very small value, which further justifies the usage of Eq. (8) throughout the asymptotic analysis. Under more asymmetrical conditions, e.g., very large (small) global equivalence ratios or very large difference between fuel and oxidizer Lewis numbers, the definition of Eq. (8) is no longer appropriate [3,27]. The alignment between tangential vector of mixture-fraction gradient and normal vector of temperature (product's mass-fraction) iso-surface plays an important role in determining the local triple flame speed. Pantano [28] has proposed a more robust definition of local triple flame speed for more general contexts during the investigation of non-premixed edge flames in turbulent lifted flame. Karami et al. [29,30] showed that the local triple flame speed is a function of propagation velocities of mixture-fraction and temperature (product-mass fraction) iso-surfaces, and iso-surface orientations at the triple point. In order to capture the axial movement relative to the local flow field, the definition in Eq. (8) should be modified accordingly for asymmetrical triple flames like Lu and Matalon [27].

3.1 Large activation energy limit

The expanding triple flame is similar to the diffusion flame disc/hole considered in previous studies [31–34]. Nayagam and coworkers [12,31,32] conducted theoretical analysis on flame disc in both premixed and diffusion flame regimes. They found that the flame disc expands at nearly constant speed at large radius. Transient simulations in the presence/absence of flow [34,35] were conducted, indicating that the propagation of triple flame can be described following quasi-steady approximation for $R_f \gg 1/\varepsilon$. In analogy to the transient formulation for expanding premixed spherical flames [36,37], the governing equations can be simplified by neglecting the time-dependent term and approximately writing $1/(\xi + \varepsilon R_f) \approx 1/\varepsilon R_f$, i.e.,

$$\begin{cases} -\left(U_f + \dfrac{1}{R_f} - \dfrac{\varepsilon\xi}{\beta^2}\right)\dfrac{\partial\theta}{\partial\xi} - \dfrac{2\varepsilon(\eta + \beta\bar{\eta}_{st})}{\beta^2}\dfrac{\partial\theta}{\partial\eta} = \varepsilon\left(\dfrac{\partial^2\theta}{\partial\xi^2} + \dfrac{\partial^2\theta}{\partial\eta^2}\right) + \dfrac{\omega}{\varepsilon}, \\ -\left(U_f + \dfrac{1}{Le_F R_f} - \dfrac{\varepsilon\xi}{\beta^2}\right)\dfrac{\partial y_F}{\partial\xi} - \dfrac{2\varepsilon(\eta + \beta\bar{\eta}_{st})}{\beta^2}\dfrac{\partial y_F}{\partial\eta} = \dfrac{\varepsilon}{Le_F}\left(\dfrac{\partial^2 y_F}{\partial\xi^2} + \dfrac{\partial^2 y_F}{\partial\eta^2}\right) - \dfrac{\omega}{\varepsilon}, \\ -\left(U_f + \dfrac{1}{Le_O R_f} - \dfrac{\varepsilon\xi}{\beta^2}\right)\dfrac{\partial y_O}{\partial\xi} - \dfrac{2\varepsilon(\eta + \beta\bar{\eta}_{st})}{\beta^2}\dfrac{\partial y_O}{\partial\eta} = \dfrac{\varepsilon}{Le_O}\left(\dfrac{\partial^2 y_O}{\partial\xi^2} + \dfrac{\partial^2 y_O}{\partial\eta^2}\right) - \dfrac{\omega}{\varepsilon}, \end{cases} \tag{9}$$

where $\bar{\eta}_{st} = \sqrt{\lambda}\, z_{st}$ is the rescaled stoichiometric surface location, and it is of order unity $O(1)$.

Similar to the work of Daou and coworkers [7–9], here we consider the asymptotic limit of large activation energy and weak strain rate, $\beta^{-1} \ll \varepsilon \ll 1$. As shown in Fig. 2, the large activation energy restricts the reaction zone into an infinitely thin layer in the limit $\beta \to \infty$, and the weak strain results in the flame preheat layer thickness being $O(\varepsilon)$. A detailed length scale analysis can be found in the previous theoretical work of Daou and Liñán [7] and therefore is not repeated here. We first consider the large activation energy limit, $\beta \to \infty$, and obtain the solution outside the reaction sheet where diffusion is balanced by convection. With appropriate jump conditions, the problem is free from the presence of β.

In analogy to the analysis proposed by Daou and Liñán [7], we presume the Lewis number to be near unity, and thereby the quantities $l_F = \beta(Le_F - 1)$ and $l_O = \beta(Le_O - 1)$ are of order 1. The dependent variables are expanded in terms of β^{-1},

$$\theta = \theta^{(0)} + \beta^{-1}\theta^{(1)} + \cdots,$$
$$y_F = y_F^{(0)} + \beta^{-1}y_F^{(1)} + \cdots, \tag{10}$$
$$y_O = y_O^{(0)} + \beta^{-1}y_O^{(1)} + \cdots.$$

Hence, the downstream boundary conditions are linearized accordingly, yielding

$$\theta = 0, \qquad y_F = 1 - \frac{\gamma_F \eta}{\beta}, \qquad y_O = 1 + \frac{\gamma_O \eta}{\beta}, \tag{11}$$

in the near flame front regime, where γ_F and γ_O are

$$\gamma_F = \frac{2\exp(-\bar{\eta}_{st}^2)}{\sqrt{\pi}(1 - \mathrm{erf}(\bar{\eta}_{st}))}, \qquad \gamma_O = \frac{2\exp(-\bar{\eta}_{st}^2)}{\sqrt{\pi}(1 + \mathrm{erf}(\bar{\eta}_{st}))}. \tag{12}$$

To the zeroth order, we have the conserved quantity in both upstream and downstream mixture, $\theta^{(0)} + y_F^{(0)} = \theta^{(0)} + y_O^{(0)} = 1$. We introduce the excess enthalpies h and k to access the flame structure of order β^{-1},

$$h = \theta^{(1)} + y_F^{(1)}, \qquad k = \theta^{(1)} + y_O^{(1)}. \tag{13}$$

Furthermore, we reformulate the problem in the flame-attached coordinate $\hat{\xi} = \xi - f(\eta)$ and $\hat{\eta} = \eta$, where $f(\eta)$ represents the prescribed characteristic premixed flame sheet. The governing equations become

$$\begin{cases} -\left(U_f + \dfrac{1}{R_f}\right)\dfrac{\partial \theta^{(0)}}{\partial \hat{\xi}} = \varepsilon \Delta \theta^{(0)}, \\ -\left(U_f + \dfrac{1}{R_f}\right)\dfrac{\partial h}{\partial \hat{\xi}} - \dfrac{l_F}{R_f}\dfrac{\partial \theta^{(0)}}{\partial \hat{\xi}} = \varepsilon \Delta h + \varepsilon l_F \Delta \theta^{(0)}, \\ -\left(U_f + \dfrac{1}{R_f}\right)\dfrac{\partial k}{\partial \hat{\xi}} - \dfrac{l_O}{R_f}\dfrac{\partial \theta^{(0)}}{\partial \hat{\xi}} = \varepsilon \Delta k + \varepsilon l_O \Delta \theta^{(0)}, \end{cases} \tag{14}$$

where the operator Δ is defined as

$$\Delta = \left(f'^2 + 1\right)\frac{\partial^2}{\partial \hat{\xi}^2} + \frac{\partial^2}{\partial \hat{\eta}^2} - 2f'\frac{\partial^2}{\partial \hat{\xi}\partial \hat{\eta}} - f''\frac{\partial}{\partial \hat{\xi}}. \tag{15}$$

The solutions of the governing equations are subject to the jump conditions

$$\left[\theta^{(0)}\right] = [h] = [k] = 0, \tag{16}$$

$$\left[\frac{\partial h}{\partial \hat{\xi}}\right] + l_F\left[\frac{\partial \theta^{(0)}}{\partial \hat{\xi}}\right] = \left[\frac{\partial k}{\partial \hat{\xi}}\right] + l_O\left[\frac{\partial \theta^{(0)}}{\partial \hat{\xi}}\right] = 0, \tag{17}$$

$$\varepsilon\sqrt{1 + f'^2}\left[\frac{\partial \theta^{(0)}}{\partial \hat{\xi}}\right] = -\left(1 + \frac{1}{2}(\mu - \sigma)\right)^{\frac{1}{2}} \exp\left(\frac{\sigma}{2}\right), \tag{18}$$

in which the notation $[\psi] = \psi\left(\hat{\xi} = 0^+, \hat{\eta}\right) - \psi\left(\hat{\xi} = 0^-, \hat{\eta}\right)$ is used. These jump conditions are the same as those reported by Daou and Liñán [7]. Besides, σ and μ take the values of h or k depending on the local equivalence ratio,

$$\begin{cases} \sigma = h\left(\hat{\xi} = 0^+, \hat{\eta}\right), \ \mu = k\left(\hat{\xi} = 0^+, \hat{\eta}\right), & k \geq h, \\ \sigma = k\left(\hat{\xi} = 0^+, \hat{\eta}\right), \ \mu = h\left(\hat{\xi} = 0^+, \hat{\eta}\right), & k < h. \end{cases} \tag{19}$$

3.2 Weak strain limit

For large activation energy in the limit $\beta \to \infty$, the reaction zone is an infinitely thin discontinuity surface. The parameter ε characterizes the ratio of the preheat zone thickness to the mixing layer thickness. In the limit of $\varepsilon \to 0$, the flame front preheat zone is a thin region of order $O(\varepsilon)$. Outside the preheat zone, both diffusion and convection are negligible. In this regime, the classical tri-branchial flame structure is observed both in numerical simulations [3,5] and experiments [6,21,38]. We conduct an asymptotic analysis in the weak strain limit and seek both the inner and outer solutions. For the outer solution, the asymptotic expansion for the temperature and excess enthalpies are written in the form

$$\begin{aligned} \theta^{(0)} &= \Theta_0 + \varepsilon\Theta_1 + \cdots, \\ h &= H_0 + \varepsilon H_1 + \cdots, \\ k &= K_0 + \varepsilon K_1 + \cdots. \end{aligned} \tag{20}$$

The flame shape function and flame propagation speed are expanded in analogous forms,

$$f = f_0 + \varepsilon f_1 + \cdots, \qquad U_f = U_{f0} + \varepsilon U_{f1} + \cdots. \tag{21}$$

After substituting the above quantities into the governing equations (14), we obtain the following outer solutions using the boundary conditions,

$$\Theta_0 = \begin{cases} 0, \\ 1, \end{cases} \quad \mathrm{H}_0 = \begin{cases} -\gamma_F \hat{\eta}, \\ -\gamma_F \hat{\eta} + A, \end{cases} \quad \mathrm{K}_0 = \begin{cases} \gamma_O \hat{\eta}, & \text{for } \hat{\xi} > 0, \\ \gamma_O \hat{\eta} + B, & \text{for } \hat{\xi} < 0. \end{cases} \tag{22}$$

The higher order solutions can also be determined and they are all essentially zero, i.e., $\Theta_1 = \mathrm{H}_1 = \mathrm{K}_1 = \Theta_2 = \mathrm{H}_2 = \mathrm{K}_2 = \cdots = 0$.

For the inner solution, we introduce the stretched coordinate $\zeta = \hat{\xi}/\varepsilon$, and the temperature and excess enthalpies are transformed into functions depending on ζ. The asymptotic expansions for the inner solution are written as

$$\begin{aligned} \theta^{(0)} &= \theta_0 + \varepsilon\theta_1 + \cdots, \\ h &= h_0 + \varepsilon h_1 + \cdots, \\ k &= k_0 + \varepsilon k_1 + \cdots. \end{aligned} \tag{23}$$

Consequently, the equations for the leading order terms are

$$\begin{cases} -\left(U_{f0} + \dfrac{1}{R_f}\right)\dfrac{\partial \theta_0}{\partial \zeta} = \mathcal{L}_0 \theta_0, \\ -\left(U_{f0} + \dfrac{1}{R_f}\right)\dfrac{\partial h_0}{\partial \zeta} - \dfrac{l_F}{R_f}\dfrac{\partial \theta_0}{\partial \zeta} = \mathcal{L}_0(h_0 + l_F\theta_0), \\ -\left(U_{f0} + \dfrac{1}{R_f}\right)\dfrac{\partial k_0}{\partial \zeta} - \dfrac{l_O}{R_f}\dfrac{\partial \theta_0}{\partial \zeta} = \mathcal{L}_0(k_0 + l_O\theta_0), \end{cases} \tag{24}$$

where $\mathcal{L}_0 = \left(f_0'^2 + 1\right)\frac{\partial^2}{\partial \zeta^2}$. Using the jump and matching conditions in equations (16)-(18) and (22), The analytical solutions for temperature and components' concentration are obtained as

$$\theta_0 = \begin{cases} e^{-\alpha\zeta}, & \zeta > 0, \\ 1 \quad, & \zeta < 0, \end{cases} \tag{25}$$

$$h_0 = \begin{cases} -\gamma_F \hat{\eta} + \dfrac{l_F\left(U_{f0}\zeta - \dfrac{1}{\alpha R_f}\right)}{{f_0'}^2 + 1} e^{-\alpha\zeta}, & \zeta > 0, \\ -\gamma_F \hat{\eta} - \dfrac{l_F}{R_f U_{f0} + 1} \qquad , & \zeta < 0, \end{cases} \tag{26}$$

$$k_0 = \begin{cases} \gamma_O \hat{\eta} + \dfrac{l_O\left(U_{f0}\zeta - \dfrac{1}{\alpha R_f}\right)}{{f_0'}^2 + 1} e^{-\alpha\zeta}, & \zeta > 0, \\ \gamma_O \hat{\eta} - \dfrac{l_O}{R_f U_{f0} + 1} \qquad , & \zeta < 0, \end{cases} \tag{27}$$

where $\alpha = \left(R_f U_{f0} + 1\right)/\left(R_f {f_0'}^2 + R_f\right)$. Using the jump relation (18) together with equations (25)-(27) we have

$$\frac{U_{f0} + \dfrac{1}{R_f}}{\sqrt{{f_0'}^2 + 1}} = \begin{cases} \sqrt{1 + \dfrac{\gamma_O + \gamma_F}{2}\hat{\eta} + \dfrac{1}{2}\dfrac{l_F - l_O}{R_f U_{f0} + 1}}\, e^{-\frac{1}{2}\left(\gamma_F \hat{\eta} + \frac{l_F}{R_f U_{f0} + 1}\right)}, & k \geq h, \\ \sqrt{1 - \dfrac{\gamma_O + \gamma_F}{2}\hat{\eta} - \dfrac{1}{2}\dfrac{l_F - l_O}{R_f U_{f0} + 1}}\, e^{\frac{1}{2}\left(\gamma_O \hat{\eta} - \frac{l_O}{R_f U_{f0} + 1}\right)}, & k \leq h. \end{cases} \tag{28}$$

The local displacement speed of triple flames refers to the normal component of local propagation speed with respect to the unburnt mixture [39] and is given as

$$\overline{U}_{f0} = \frac{U_{f0}}{\sqrt{1 + {f_0'}^2}} \tag{29}$$

and it is maximum when $f_0'(\hat{\eta}^*) = 0$, where $\hat{\eta}^*$ denotes the leading edge position. Exploiting this condition, we find that

$$\hat{\eta}^* = \begin{cases} \dfrac{1}{\gamma_O + \gamma_F}\left(\dfrac{\gamma_O - \gamma_F}{\gamma_F} - \dfrac{l_F - l_O}{R_f U_{f0} + 1}\right), & \phi \leq 1, \\ \dfrac{1}{\gamma_O + \gamma_F}\left(\dfrac{\gamma_O - \gamma_F}{\gamma_O} - \dfrac{l_F - l_O}{R_f U_{f0} + 1}\right), & \phi \geq 1, \end{cases} \tag{30}$$

at which the local flame speed satisfies

$$U_{f0}+\frac{1}{R_f}=\begin{cases}\sqrt{\dfrac{\gamma_O+\gamma_F}{2\gamma_F}}\exp\left(\dfrac{\gamma_F-\gamma_O-\dfrac{\gamma_O l_F+\gamma_F l_O}{R_f U_{f0}+1}}{2(\gamma_O+\gamma_F)}\right), & \phi\le 1,\\ \sqrt{\dfrac{\gamma_O+\gamma_F}{2\gamma_O}}\exp\left(\dfrac{\gamma_O-\gamma_F-\dfrac{\gamma_O l_F+\gamma_F l_O}{R_f U_{f0}+1}}{2(\gamma_O+\gamma_F)}\right), & \phi\ge 1.\end{cases} \tag{31}$$

Substitute the equation (31) back into the equation (28), and the first order derivative of flame shape function $f_0'(\eta)$ is therefore obtained. Then the shape of the flame front is readily obtained after integration of $f_0'(\eta)$.

We consider the case of unity initial global equivalence ratio (i.e., $\phi = 1$), for which U_{f0} is readily obtained as

$$U_{f0}+\frac{1}{R_f}=\exp\left(-\frac{l_F+l_O}{4\left(R_f U_{f0}+1\right)}\right). \tag{32}$$

The above expression describes the change of the displacement speed U_{f0} with the azimuthal curvature $1/R_f$ and its dependence on Lewis numbers under the limit of weak strain rate. We fix the Lewis number of the oxidizer to be unity, and only change the fuel Lewis number. Equation (32) is solved numerically with for $\beta = 10$, and the results are depicted on Fig. 3 for different fuel Lewis numbers. It is seen that U_{f0} is linearly proportional to $1/R_f$ for large radius. The non-monotonic response of U_{f0} to $1/R_f$ are observed for sufficiently small fuel Lewis number. Similar non-monotonic change with respect to strain rate was also observed in the literature [7].

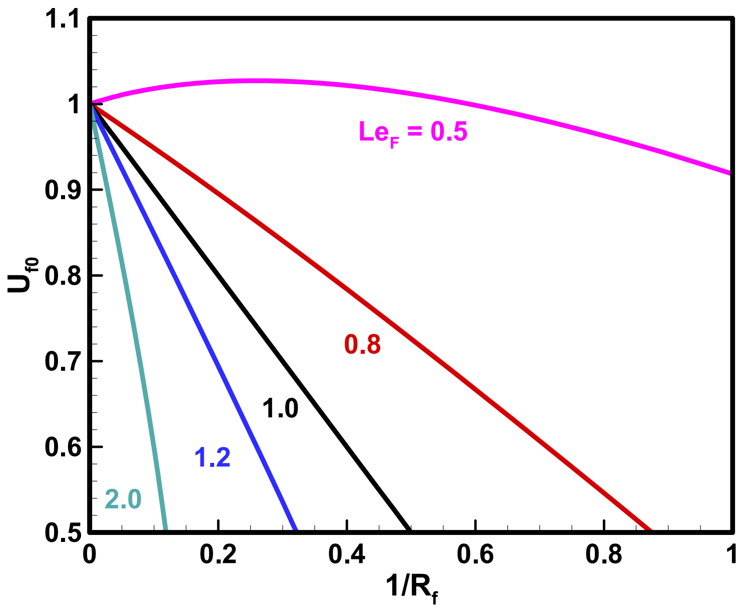

Fig. 3 Change of displacement speed U_{f0} with the azimuthal curvature $1/R_f$ for different fuel Lewis numbers but the same oxidizer Lewis number of $Le_O = 1$. Here we fix $\beta = 10$.

In fact, for sufficiently large radius $R_f \gg 1$, equation (32) reduces to

$$U_{f0} \approx 1 - \left(1 + \frac{l_F + l_O}{4}\right)\frac{1}{R_f} + O\left(\frac{1}{R_f}\right). \tag{33}$$

The second-order derivative $f_0''(\hat{\eta}^*)$ is evaluated by differentiating the equation (28) at the leading edge for further use, providing

$$f_0''(\hat{\eta}^*) = \begin{cases} -\dfrac{\gamma_F}{\sqrt{2}}, & \phi \le 1, \\ -\dfrac{\gamma_O}{\sqrt{2}}, & \phi \ge 1. \end{cases} \tag{34}$$

This quantity can be used to determine the transverse curvature $1/R_t$. With proper coordination transformation from the flame attached coordinate $(\hat{\xi}, \hat{\eta})$ to the original coordinate (r, z), we have $1/R_t = -\varepsilon f_0''$. For the case $\phi = 1$, we have $\gamma_F = \gamma_O = 2/\sqrt{\pi}$ according to equation (12), and hence $1/R_t = \varepsilon\sqrt{2/\pi}$.

The influence of strain rate is absent in the zeroth-order approximation to the triple flame propagation speed, given in equation (33). This implies that higher order terms of $O(\varepsilon)$ must be considered. The corresponding equations are given by,

$$
\begin{cases}
-\left(U_{f0}+\dfrac{1}{R_f}\right)\dfrac{\partial \theta_1}{\partial \zeta}=\mathcal{L}_0\theta_1+\mathcal{L}_1\theta_0+U_{f1}\dfrac{\partial \theta_0}{\partial \zeta}, \\
-\left(U_{f0}+\dfrac{1}{R_f}\right)\dfrac{\partial h_1}{\partial \zeta}-\dfrac{l_F}{R_f}\dfrac{\partial \theta_1}{\partial \zeta}=\mathcal{L}_0(h_1+l_F\theta_1)+\mathcal{L}_1(h_0+l_F\theta_0)+U_{f1}\dfrac{\partial h_0}{\partial \zeta}, \\
-\left(U_{f0}+\dfrac{1}{R_f}\right)\dfrac{\partial k_1}{\partial \zeta}-\dfrac{l_O}{R_f}\dfrac{\partial \theta_1}{\partial \zeta}=\mathcal{L}_0(k_1+l_O\theta_1)+\mathcal{L}_1(k_0+l_O\theta_0)+U_{f1}\dfrac{\partial k_0}{\partial \zeta},
\end{cases}
\tag{35}
$$

in which the operator $\mathcal{L}_1$ is defined as

$$
\mathcal{L}_1=2f_0'f_1'\frac{\partial^2}{\partial \zeta^2}-2f_0'\frac{\partial^2}{\partial \zeta \partial \hat{\eta}}-f_0''\frac{\partial}{\partial \zeta}. \tag{36}
$$

These equations are valid except for the flame surface. The jump condition at $\zeta=0$ is determined based on equation (16)-(18),

$$
[\theta_1]=[h_1]=[k_1]=0, \tag{37}
$$

$$
\left[\frac{\partial h_1}{\partial \zeta}\right]+l_F\left[\frac{\partial \theta_1}{\partial \zeta}\right]=\left[\frac{\partial k_1}{\partial \zeta}\right]+l_O\left[\frac{\partial \theta_1}{\partial \zeta}\right]=0, \tag{38}
$$

$$
\left[\frac{\partial \theta_1}{\partial \zeta}\right]=\left(\frac{\sigma_1}{2}-\frac{f_0'f_1'}{f_0'^2+1}+\frac{\dfrac{\mu_1-\sigma_1}{4}}{1+\dfrac{\mu_0-\sigma_0}{2}}\right)\left[\frac{\partial \theta_0}{\partial \zeta}\right]. \tag{39}
$$

Upstream of the flame surface, the flame temperature is bounded, which eliminates the exponential terms. Meanwhile, to match with the outer solution in equation (25), the upstream solution for θ_1 is $\theta_1=0$ for $\zeta\geq 0$. Solving the equation (35) in the unburnt gas with the jump conditions in equations (37)-(38), and matching with the high order outer solutions, i.e., $\Theta_1=\mathrm{H}_1=\mathrm{K}_1=0$, it is readily obtained that

$$
\theta_1=\frac{1}{f_0'^2+1}\left(\frac{2\alpha f_0'^2 f_0''}{f_0'^2+1}\zeta-U_{f1}+f_0''+2\alpha f_0'f_1'\right)\zeta e^{-\alpha\zeta}, \tag{40}
$$

$$h_1 = \frac{l_F R_f e^{-\alpha\zeta}}{R_f U_{f0} + 1}\left(\frac{U_{f1} + R_f U_{f0} f_0''}{R_f U_{f0} + 1}\right) + \frac{l_F \zeta e^{-\alpha\zeta}}{f_0'^2 + 1}\left(\frac{U_{f1} - f_0''}{R_f U_{f0} + 1} + U_{f1} - 2\alpha f_0' f_1'\right)$$

$$+ \frac{l_F \zeta^2 e^{-\alpha\zeta}}{\left(f_0'^2 + 1\right)^2}\left(2\alpha f_0' f_1' U_{f0} + 2\alpha f_0'' - U_{f0} U_{f1} - f_0'' U_{f0} - \frac{2 f_0''}{R_f}\right) \tag{41}$$

$$+ \frac{2 l_F \alpha f_0'^2 f_0'' U_{f0} \zeta^3 e^{-\alpha\zeta}}{\left(f_0'^2 + 1\right)^3},$$

$$k_1 = \frac{l_O R_f e^{-\alpha\zeta}}{R_f U_{f0} + 1}\left(\frac{U_{f1} + R_f U_{f0} f_0''}{R_f U_{f0} + 1}\right) + \frac{l_O \zeta e^{-\alpha\zeta}}{f_0'^2 + 1}\left(\frac{U_{f1} - f_0''}{R_f U_{f0} + 1} + U_{f1} - 2\alpha f_0' f_1'\right)$$

$$+ \frac{l_O \zeta^2 e^{-\alpha\zeta}}{\left(f_0'^2 + 1\right)^2}\left(2\alpha f_0' f_1' U_{f0} + 2\alpha f_0'' - U_{f0} U_{f1} - f_0'' U_{f0} - \frac{2 f_0''}{R_f}\right) \tag{42}$$

$$+ \frac{2 l_O \alpha f_0'^2 f_0'' U_{f0} \zeta^3 e^{-\alpha\zeta}}{\left(f_0'^2 + 1\right)^3}.$$

We now consider the remaining jump condition (39) and determine the next order approximation for triple-flame speed

$$\frac{R_f\left(U_{f1} - f_0''\right)}{R_f U_{f0} + 1} = \frac{f_0' f_1'}{f_0'^2 + 1} + \frac{\sigma_1}{2} + \frac{\frac{\mu_1 - \sigma_1}{4}}{1 + \frac{\mu_0 - \sigma_0}{2}}. \tag{43}$$

Despite the flame shape function in equation (43) being unknown, it is still possible to determine the flame propagation speed at the leading edge, where $f_0'(\hat{\eta}^*) = 0$. Accordingly, we have,

$$U_{f1} = \begin{cases} -\frac{\gamma_F}{\sqrt{2}}\left(1 + \frac{\frac{1}{2}\frac{\gamma_F l_O + \gamma_O l_F}{\gamma_O + \gamma_F}}{1 - \frac{1}{2}\frac{\gamma_F l_O + \gamma_O l_F}{\gamma_O + \gamma_F}\frac{1}{R_f U_{f0} + 1}}\right), & \phi \le 1, \\ -\frac{\gamma_O}{\sqrt{2}}\left(1 + \frac{\frac{1}{2}\frac{\gamma_F l_O + \gamma_O l_F}{\gamma_F + \gamma_O}}{1 - \frac{1}{2}\frac{\gamma_F l_O + \gamma_O l_F}{\gamma_F + \gamma_O}\frac{1}{R_f U_{f0} + 1}}\right), & \phi \ge 1. \end{cases} \tag{44}$$

In the limit of unity global equivalence ratio (i.e., $\phi = 1$), equation (44) can be simplified to

$$U_{f1} = -\sqrt{\frac{2}{\pi}}\left(1 + \frac{\frac{l_F + l_O}{4}}{1 - \frac{l_F + l_O}{4}\frac{1}{R_f U_{f0} + 1}}\right), \tag{45}$$

The asymptotic form for the triple flame displacement speed, for the case of $\phi = 1$, are defined as $U_f = U_{f0} + \varepsilon U_{f1}$. Substituting the results for the leading and first order terms in equations (33) and (45), we have, for $R_f \gg 1$,

$$U_f = 1 - \left(1 + \frac{l_F + l_O}{4}\right)\left(\frac{1}{R_f} + \frac{1}{R_t}\right), \qquad \text{with } \frac{1}{R_t} = \sqrt{\frac{2}{\pi}}\varepsilon, \tag{46}$$

where $1/R_t = \varepsilon\sqrt{2/\pi}$ is obtained from equation (34) as mentioned before.

The present formulation extends that given by Daou and coworkers [7–9] by considering the effect of the flame radius, R_f. The present theory is consistent with that obtained by Daou and coworkers [7–9] in the limit of large triple flame radius. Equation (46) implies that the azimuthal flame curvature $1/R_f$ has considerable impact on the displacement speed of the triple flame in addition to the local flame curvature $1/R_t$, and that the resulting U_f depends on the total flame curvature, $1/R_f + 1/R_t$, at the leading edge (which is equal to twice the mean curvature). The Lewis number also affects the triple flame speed since it changes the excess enthalpy near the flame edge.

4. Numerical study

To validate the theoretical analysis under the quasi-steady assumption and large-activation-energy limit, two-dimensional simulations considering finite activation energy are conducted. Two types of simulations are carried out: one is the transient simulation of the propagation of the expanding triple flame induced by a hot spot at the stagnation point, and the other is the steady solution for the triple flame in a coordinate system fixed on the propagating flame front in which the displacement speed is obtained by numerically solving an eigenvalue problem. These two types of simulations and corresponding results are addressed in subsection 4.1 and 4.2. In all simulations, we use for the parameters the fixed values $\beta = 10$, $\alpha_h = 0.85$, $Le_O = 1.0$ and $\phi = 1.0$.

4.1 The transient propagation of the expanding triple flame

We first simulate the initiation and propagation of an expanding triple flame induced by a hot spot in a counterflow as depicted in Fig. 1. The propagation speed of the expanding triple flame can be determined in terms of the parameters β, α_h, Le_F, Le_O and λ. The numerical methods are the same as those in our previous work [24]. The governing equations are solved using finite difference methods within a two-dimensional computation domain of $[0, r_m] \times [-z_m^-, z_m^+]$. The first- and second-order spatial derivatives in the governing equations are discretized using the sixth-order compact scheme for the internal grids. As for grids near the boundaries, the third-order one-sided compact scheme is adopted. The discretized governing equations are first-order ordinary differential equations with respect to time, which is integrated using the explicit second-order Runge–Kutta method. For ease of boundary treatment, we adopt a slightly different scaling for the mass fraction of fuel and oxidizer, $\bar{y}_F = Y_F/Y_{Fu}$ and $\bar{y}_O = Y_O/Y_{Ou}$ respectively. The triple flame position is determined as the radial location of the maximal of the reaction rate. The displacement speed of the expanding triple flame is equal to the difference between the flame front speed, dR_f/dt, and the local flow velocity, λR_f, i.e., $U_f = dR_f/dt - \lambda R_f$.

The transient evolution of the expanding triple flame is shown in Fig. 4 for the strain rate of $\lambda = 0.01$ and fuel Lewis number of $Le_F = 1$. The hot spot has the initial radius $R_i = 1.4$ and temperature $\theta_i = 1$. Intense chemical reactions are induced by the hot spot, and an expanding triple flame is established around $R_f = 2$. As the flame propagates outwards, the influence of the initial ignition kernel decays and the propagation becomes self-sustained in the case of successful ignition. Figure 4 shows that the flame structure remains nearly the same for $R_f = 5$, 10 and 20, indicating that the expanding triple flame propagates in a quasi-steady manner for $R_f > 5$.

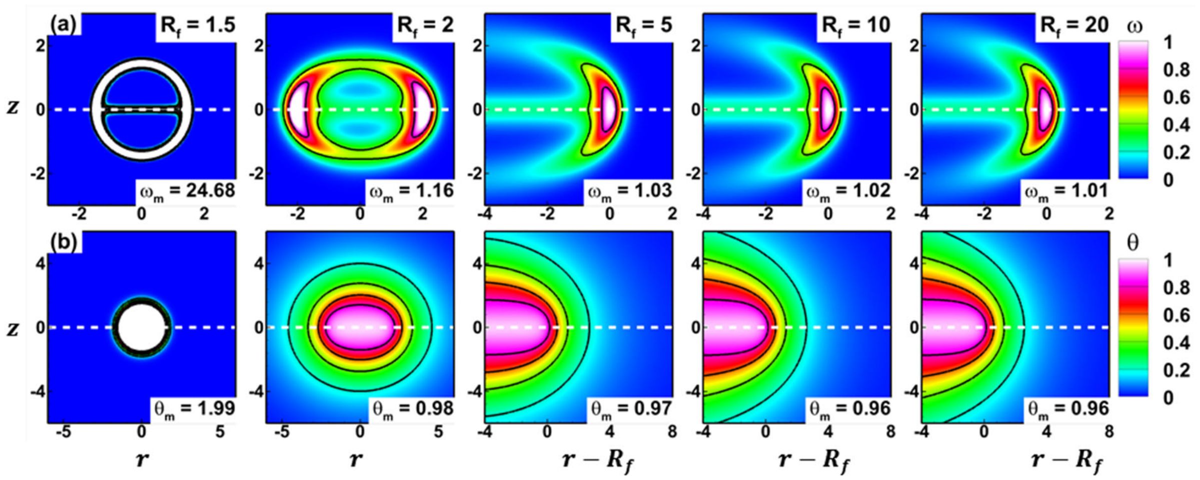

Fig. 4 Evolution of the (a) reaction rate ω and (b) temperature θ contours during the initiation and propagation of the expanding tripe flame induced by a spherical hot spot with radius $R_i = 1.4$ and temperature $\theta_i = 1$. The strain rate is $\lambda = 0.01$ and the fuel Lewis numbers is $Le_F = 1$. Note that $r - R_f$ instead of r is used for the horizontal axis when $R_f \geq 5$.

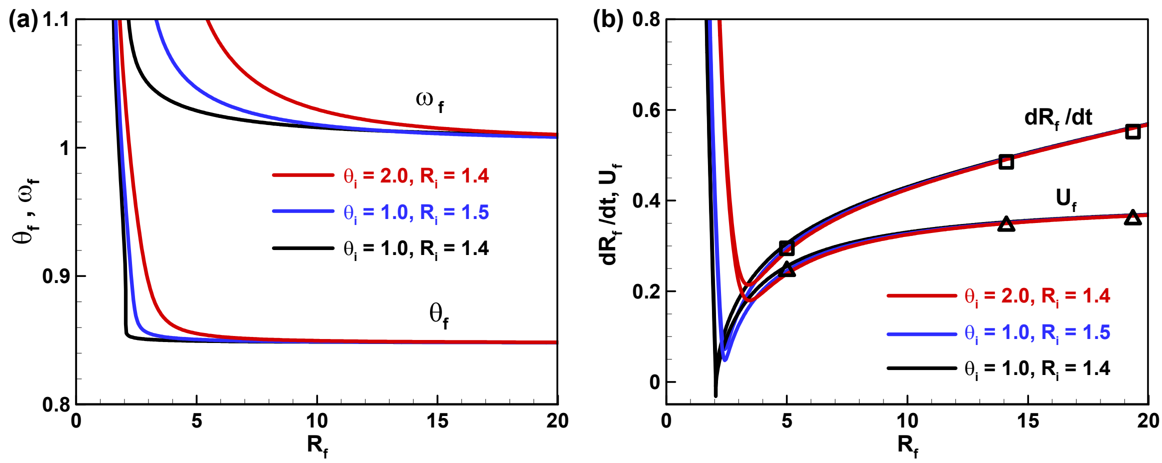

Fig. 5 (a) Change of temperature θ_f and reaction rate ω_f at the triple point and (b) change of the absolute propagation speed, dR_f/dt, and displacement speed, U_f, of the expanding triple flame with the flame radius R_f for $\lambda = 0.01$ and $Le_F = 1$. The symbols denote results from the steady solution of the eigenvalue problem obtained in a frame attached to the flame front as described in section 4.2.

Different ignition parameters are considered to test the universality of the above quasi-steady propagation behavior. Figure 5(a) compares the change of temperature θ_f and reaction rate ω_f at the triple point with the flame radius for three sets of ignition parameters. The ignition parameters are seen to have significant impacts on the triple flame temperature and reaction rate at small radius. As the triple flame expands to large radius, the temparature and reaction rate practically approach constant values around the flame front regardless of the ignition parameters. The flame temperature is shown to remain constant for $R_f > 5$, while the reaction rate is more sensitive to initial conditions due to its exponential dependence on temperature according to the Arrhenius law. All curves are seen to collapse together onto a single curve for $R_f > 10$, indicating the generality of the quasi-steady propagation. The absolute propagation speed and displacement speed of the expanding triple flames are compared in Fig. 5(b). It's observed that the solutions are independent of the ignition conditions for large radius. Therefore, regardless of the initial ignition conditions leading to successful ignition, the expanding triple flame eventually propagates in a quasi-steady manner.

4.2 The steady triple flame in a frame attached to the propagating flame front

To further validate the quasi-steady assumption, we simulate the steady triple flame in a frame fixed to the propagating flame front. This allows the displacement speed to be obtained by solving numerically an eigenvalue problem. The eigenvalue problem is governed by the time independent version of equations (7). The convection and diffusion terms are discretized with upwind scheme and central difference scheme respectively, forming a system of algebraic equations. We seek the numerical solution of equations (7) with a straightforward relaxation method. Appropriate guessed temperature and reactants profiles (typically from the transient simulation) are chosen as initial conditions to accelerate the iterations. We employ the flame-controlling technique [40] to fix the flame front location. The eigenvalue, U_f, is updated at the controlling point at each iteration.

The importance of the unsteady effects can be quantified by comparing the steady solution with the transient simulation results for the same flame radius R_f. Figure 6 shows the temperature and reaction rate fields and iso-lines from both the steady solution of the eigenvalue problem and the transient simulation when $R_f = 5$ and $\lambda = 0.01$. Almost identical results are obtained from the steady solution and the transient simulation, indicating that the neglect of the unsteady terms is appropriate.

This lends reasonable justification to the quasi-steady state assumption used in the asymptotic analysis.

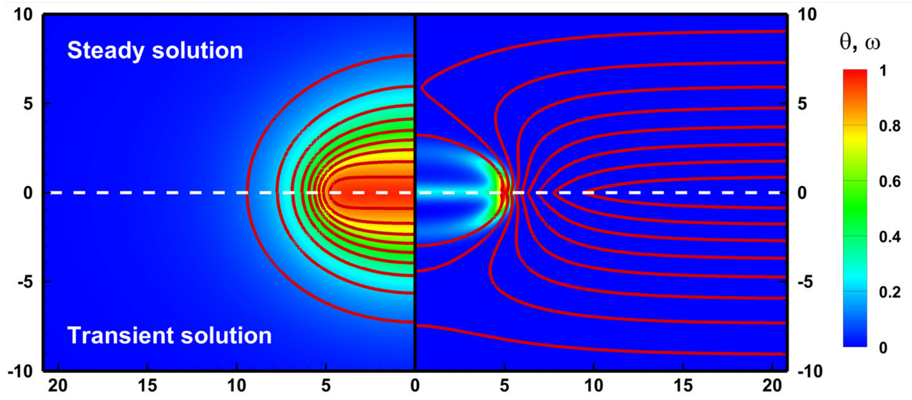

Fig. 6 Temperature (left) and reaction rate (right) fields and iso-lines from the steady solution of the eigenvalue problem (top) and the transient simulations (bottom) for $R_f = 5$, $\lambda = 0.01$ and $Le_F = Le_O = 1$.

Besides the typical case shown in Fig. 5, steady solutions for different flame radii and different strain rates are obtained and compared with transient simulation results. For example, the symbols in Fig. 5(b) denote results from steady solution with relative error below 10^{-6}. It's seen that the steady solutions agree well with those from the transient simulations. This further demonstrates that the quasi-steady assumption used in the asymptotic analysis is plausible.

Following a similar procedure, the displacement speeds of the triple flame can be determined for different strain rates. A comparison between the asymptotic results and those computed numerically from equations (7) for the case $Le_F = 1$ is shown in Fig. 7. The asymptotic results use the two-term expansion for unity Lewis numbers, $U_f + 1/R_f = 1 - \sqrt{2/\pi}\varepsilon$, given by equation (46) with l_F and l_O equal to zero. Qualitative agreement is observed at weak strain rates and large flame radius, e.g., $R_f = 5$, 10 and ∞. For larger values of the strain rates, the linear dependence on ε no longer applies as expected. We also note that for R_f above 10, the numerical results are identical regardless of the flame radius, corresponding to the solution of equation (9). The triple flame displays then a quasi-planar structure, which lends support to the quasi-planar assumption adopted in the asymptotic analysis.

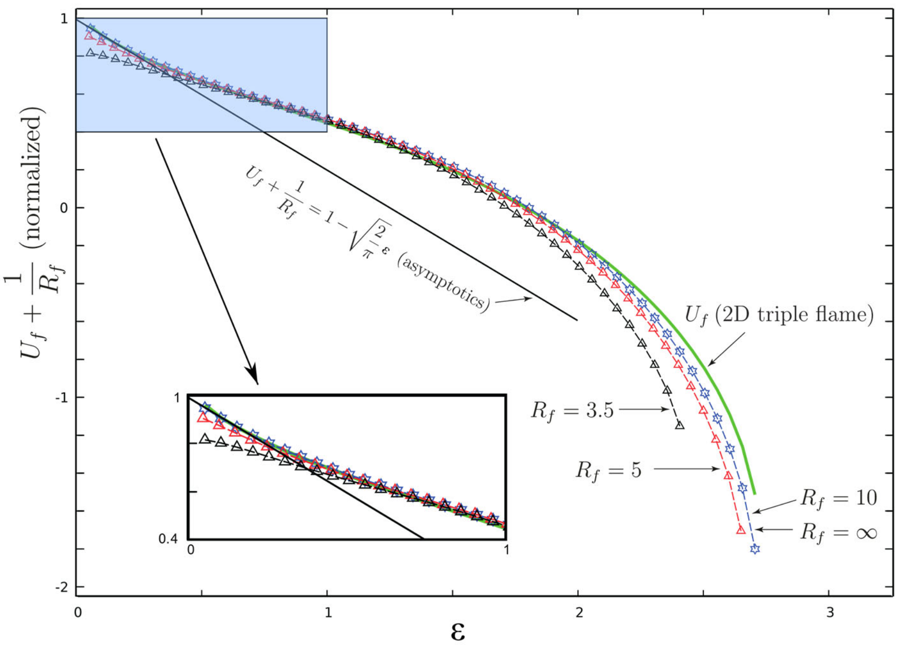

Fig. 7 $U_f + 1/R_f$ versus ε for $Le_F = 1.0$. The black, red and blue lines with symbols are obtained by solving equations (7) without the unsteady terms, while the green line corresponds to the propagation speed U_f of the two-dimensional planar triple flame as in Daou and Liñán [7]. The coordinates are normalized by the planar stoichiometric flame speed which is determined numerically to be equal to 0.793.

The two-dimensional triple flame, addressed in detail by Daou and coworkers [7–9], is also shown as the green line in Fig. 7. It is seen that the green curve is a good approximation to the curves $U_f + 1/R_f$ versus ε for all values of ε up to near extinction values, provided $R_f > 5$ approximately. It is worth pointing out that in the limit of large R_f, the main difference between the two-dimensional triple flame (green curve) and the axisymmetric triple flame considered in this paper is associated with the local radial flow, the term $\varepsilon/\beta^2(\partial/\partial\xi)$ in equation (9). These terms are expected to play a role only near extinction conditions. Although the verification is conducted only for unity Lewis number, the general quasi-steady and quasi-planar assumptions are expected to apply at least for mixtures with near-unity Lewis numbers.

4.3 Effects of stain rate and Lewis number on the triple flame propagation

In this subsection, we further investigate the effects of the curvature $1/R_f$ on the displacement speed of the expanding triple flame through transient simulation. Different strain rates and fuel Lewis numbers are considered. To be consistent with the asymptotic analysis, low strain rate and near-unity Lewis numbers are considered in the transient simulations. Figure 8(a) depicts the change of the displacement speed U_f with the azimuthal flame curvature $1/R_f$ at selected values of the strain rates of $\lambda = 0.01$, 0.05 an 0.10 for unity fuel Lewis number. The transient flame evolution process can be roughly classified into two regimes: the unsteady transition regime and the quasi-steady propagation regime. The flame is subjected to the influence of the initial ignition kernel during the first stage. Similar flame deceleration phenomena are also identified in the forced ignition in a non-premixed couterflow [24]. The quasi-steady propagation regime is analyzed in this wok. Regardless of the values of the strain rate, U_f changes linearly with $1/R_f$ in the quasi-steady propagation regime and the slopes are nearly independent of the strain rate. These normalized slopes are evaluated at later stage using the least square method, yielding 0.99, 1,00 and 1.05 respectively.

The results for different fuel Lewis numbers but the same strain rate $\lambda = 0.01$ are plotted in Fig. 8(b). It's noted that for the case of unequal fuel and oxidizer Lewis number, the triple flame becomes asymmetrical. The relative movements along the axial direction are evaluated accordingly, yields axial flame speed of the order of $O(10^{-2})$. The axial movement is negligible compared to the radical flame movement. Therefore, it's a good approximation to use equation (8) to evaluate the triple flame speed in this work. It is seen in Fig. 8(b) that the triple flame is greatly influence by the initial conditions (or namely ignition conditions) at initial stage. For mixtures with smaller fuel Lewis number, successful ignition is more easily achieved by smaller initial ignition radius, and the triple flame may propagate faster, leaving a shorter residual time for the influence of the initial conditions to decay. As shown in Fig. 8(b), a non-linear response is still observed after the inflection point $(1/R_f = 0.75)$ for the case of $Le_F = 0.8$. Similar trends are observed in the forced ignition of premixed flames in a static mixture [41-43].

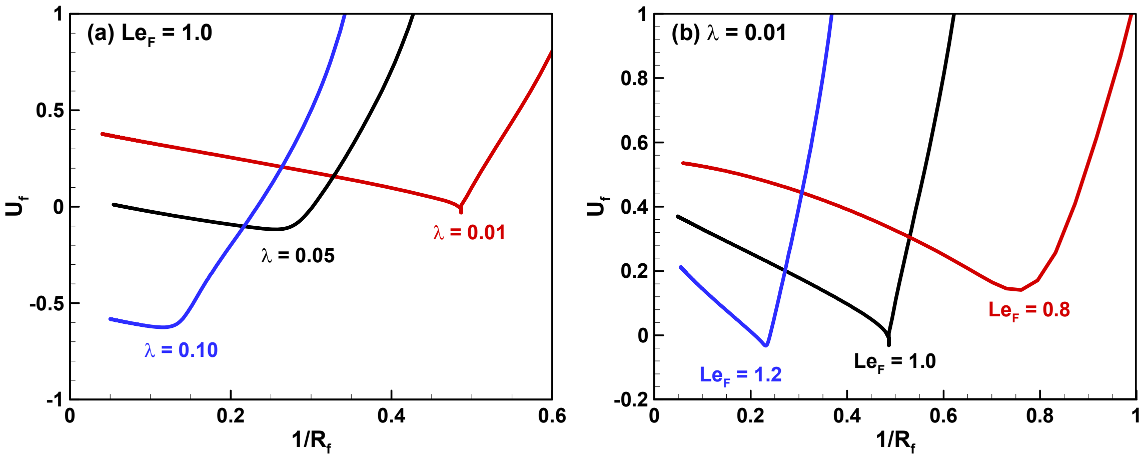

Fig. 8 Change of the displacement speed, U_f, with the flame curvature, $1/R_f$, for (a) different strain rates but the same fuel Lewis number of $Le_F = 1$ and (b) different fuel Lewis numbers but the same strain rate of $\lambda = 0.01$.

The flame propagates to a large radius and then enter the quasi-steady regime. For $1/R_f < 0.2$, the linear dependence of triple flame speed on azimuthal curvature is observed regardless of the fuel Lewis number. The preferential diffusion, quantified with Lewis number, acts as an amplifier of the impact of curvature. It is seen that the displacement speed is more sensitive to azimuthal curvature at relatively larger fuel Lewis number such as for $Le_F = 1.2$, which is consistent with the theoretical formula (46). The normalized slopes are also evaluated using the least square method for Le_F equal to 0.8 and 1.2, yielding 0.43 and 1.81 respectively. There do exist quantitative differences between numerical simulations and theoretical predictions, which is possibly due to the deviation of Lewis number from unity. However, the main conclusion in predicting the general trend for Lewis number still holds qualitatively.

5. Inwardly propagating triple flames with negative azimuthal curvature

The above analysis is performed for expanding triple flames with positive azimuthal curvature. There also exists a shrinking flame holes, in which the triple flame propagates inwardly with negative azimuthal curvature [34,35]. Here we also derive the relationship between triple flame speed and curvature for the inwardly propagating triple flames. In contrast to the expanding triple flame, the local triple flame speed of the inwardly propagating triple flame takes an opposed sign, i.e.,

$$U_f = -\frac{dR_f}{dt} + \lambda R_f = -\frac{dR_f}{dt} + \frac{\varepsilon^2}{\beta^2} R_f. \tag{47}$$

Detailed theoretical derivation procedure is similar to that presented in Sec. 3, and hence not repeated here. Analytical expressions for local triple flame speeds of inwardly propagating triple flames can be obtained as

$$U_{f0} - \frac{1}{R_f} = \begin{cases} \sqrt{\dfrac{\gamma_O + \gamma_F}{2\gamma_F}} \exp\left(\dfrac{\gamma_F - \gamma_O + \dfrac{\gamma_O l_F + \gamma_F l_O}{R_f U_{f0} - 1}}{2(\gamma_O + \gamma_F)} \right), & \phi \le 1, \\ \sqrt{\dfrac{\gamma_O + \gamma_F}{2\gamma_O}} \exp\left(\dfrac{\gamma_O - \gamma_F + \dfrac{\gamma_O l_F + \gamma_F l_O}{R_f U_{f0} - 1}}{2(\gamma_O + \gamma_F)} \right), & \phi \ge 1, \end{cases} \tag{48}$$

$$U_{f1} = \begin{cases} -\dfrac{\gamma_F}{\sqrt{2}} \left(1 + \dfrac{\dfrac{1}{2} \dfrac{\gamma_F l_O + \gamma_O l_F}{\gamma_O + \gamma_F}}{1 + \dfrac{1}{2} \dfrac{\gamma_F l_O + \gamma_O l_F}{\gamma_O + \gamma_F} \dfrac{1}{R_f U_{f0} - 1}} \right), & \phi \le 1, \\ -\dfrac{\gamma_O}{\sqrt{2}} \left(1 + \dfrac{\dfrac{1}{2} \dfrac{\gamma_F l_O + \gamma_O l_F}{\gamma_F + \gamma_O}}{1 + \dfrac{1}{2} \dfrac{\gamma_F l_O + \gamma_O l_F}{\gamma_F + \gamma_O} \dfrac{1}{R_f U_{f0} - 1}} \right), & \phi \ge 1. \end{cases} \tag{49}$$

Similar expressions for expanding triple flame discs are described by equations (31) and (44) in Section 3. The leading order solution of triple flame speed, U_{f0}, represents the role of azimuthal curvature, and is identical to that for expanding triple flame discs when the sign of U_{f0} is changed. The first order solution of triple flame speed, U_{f1}, represents the effects of mixing layer thickness, and is essentially same as that for expanding triple flame discs.

In the limit case of unity initial global equivalence ratio (i.e., $\phi = 1$) and sufficiently large radius $R_f \gg 1$, the local triple flame speed is hence simplified into

$$U_f = U_{f0} + \varepsilon U_{f1} = 1 - \left(1 + \frac{l_F + l_O}{4} \right) \left(-\frac{1}{R_f} + \frac{1}{R_t} \right), \quad \text{with } \frac{1}{R_t} = \sqrt{\frac{2}{\pi}} \varepsilon, \tag{50}$$

The above expression is equivalent to the that for expanding triple flame discs with positive the azimuthal curvature. Equations (46) and (50) imply that the propagating characteristics of triple flame depend on the total curvature at leading edge. Coupling with preferential diffusion, the positive and negative azimuthal flame curvatures lead to the excess enthalpy across the flame front and hence affect the triple flame speed in the same manner. Therefore, the sign of azimuthal curvature does not change the linear relationship between total curvature and triple flame speed.

6. Conclusion

We have carried out an asymptotic analysis addressing triple flame propagation in an axisymmetric counterflow of fuel against oxidizer. To make the analysis tractable we have adopted a thermo-diffusive model with a one-step irreversible reaction. The analysis has been performed in the limit of large activation energy and weak strain rate. An explicit formula for the displacement speed of the expanding triple flame has been derived. The formula quantifies the effects of both the flame front curvature $1/R_t$ associated with the variation in the reactant concentrations transverse to the mixing layer and the azimuthal curvature $1/R_f$ where R_f is the front leading edge radial distance from the origin. As the triple flame expands to moderately large values of R_f, the quasi-steady state is reached and the flame displacement speed is found to be linearly proportional to $1/R_f + 1/R_t$ (equal to twice the front mean curvature). In the limit of large values of R_f, the present theory is consistent with previous work by Daou and Liñán [7].

Two-dimensional axisymmetric numerical simulations have been performed to validate the quasi-steady asymptotic analysis and to extend the study to arbitrary values of the strain rate. The results from transient simulations of the expanding triple flame are compared to the steady solution of the eigen boundary value problem obtained in a frame attached to the propagating front under a quasi-steady assumption. Following a transient ignition phase which depends on the initial conditions, the expanding triple flame is found to propagate in a quasi-steady manner independent of the latter when $R_f > 5$, approximately. Although the theoretical analysis is performed in the weak strain limit, the linear dependence of the triple flame speed on the curvature $1/R_f$ is found to be applicable over a wide range of strain rates. The inwardly propagating triple flame holes with negative azimuthal curvature are also considered and an explicit analytical expression for local triple flame speed is derived. The triple flame speed depends primarily on the overall curvature at triple point, which further extends the applicability of present analysis.

Here we have considered the case of unity initial global equivalence ratio (i.e., $\phi = 1$) for simplicity. For practical applications involving undiluted hydrocarbon-air mixtures, we have typically $\phi \gg 1$, for which the diffusion flame branch merges with the lean premixed branch and thereby the partially premixed flame loses its tri-brachial structure [44]. In future works, it would be interesting to examine the influence of stoichiometry on the displacement speed of the expanding triple flame. Furthermore, it would be interesting in future simulations to take into account momentum equations and variable density so that the effects of thermal expansion on expanding triple flames can be assessed. The quasi-steady assumption may not hold for large the azimuthal curvature and the transient effect (or memory effect) [45] on initial ignition kernel development in a counterflow needs to be assessed in future analysis.

Declaration of Competing Interest

The authors declare no conflict of interest.

Acknowledgements

This research was funded by National Natural Science Foundation of China (Nos. 52176096 and 51861135309) and the UK EPSRC grant EP/V004840/1.

References

[1] E. Mastorakos, Forced ignition of turbulent spray flames, *Proc. Combust. Inst.* 36 (2017), 2367–2383.

[2] L. Vervisch and T. Poinsot, Direct numerical simulation of non-premixed turbulent flames, *Annu. Rev. Fluid Mech.* 30 (1998), 655–691.

[3] S.H. Chung, Stabilization, propagation and instability of tribrachial triple flames, *Proc. Combust. Inst.* 31 (2007), 877–892.

[4] J. Buckmaster, Edge-flames, *Prog. Energy Combust. Sci.* 28 (2002), 435–475.

[5] G.R. Ruetsch, L. Vervisch and A. Liñán, Effects of heat release on triple flames, *Phys. Fluids* 7 (1995), 1447–1454.

[6] S.H. Chung and B.J. Lee, On the characteristics of laminar lifted flames in a nonpremixed jet, *Combust. Flame* 86 (1991), 62–72.

[7] J. Daou and A. Liñán, The role of unequal diffusivities in ignition and extinction fronts in strained mixing layers, *Combust. Theory Model.* 2 (1998), 449–477.

[8] R. Daou, J. Daou and J. Dold, Effect of volumetric heat loss on triple-flame propagation, *Proc. Combust. Inst.* 29 (2002), 1559–1564.

[9] R. Daou, J. Daou and J. Dold, The effect of heat loss on flame edges in a non-premixed counterflow within a thermo-diffusive model, *Combust. Theory Model.* 8 (2004), 683–699.

[10] S. Ali and J. Daou, Effect of the reversibility of the chemical reaction on triple flames, *Proc. Combust. Inst.* 31 (2007), 919–927.

[11] S. Ghosal and L. Vervisch, Stability diagram for lift-off and blowout of a round jet laminar diffusion flame, *Combust. Flame* 124 (2001), 646–655.

[12] V. Nayagam and F.A. Williams, Curvature effects on edge-flame propagation in the premixed-flame regime, *Combust. Sci. Technol.* 176 (2004), 2125–2142.

[13] W. Carnelljr and M. Renfro, Stable negative edge flame formation in a counterflow burner, *Combust. Flame* 141 (2005), 350–359.

[14] S.W. Grib and M.W. Renfro, Energy analysis of unsteady negative edge flames in a periodic flow, *Combust. Flame* 215 (2020), 113–123.

[15] D.K. Dalakoti, A. Krisman, B. Savard, A. Wehrfritz, H. Wang, M.S. Day et al., Structure and propagation of two-dimensional, partially premixed, laminar flames in diesel engine conditions, *Proc. Combust. Inst.* 37 (2019), 1961–1969.

[16] J. Carpio, P. Rajamanickam, A.L. Sánchez and F.A. Williams, Near-limit h2-o2-n2 combustion in nonpremixed counterflow mixing layers, *Combust. Flame* 216 (2020), 426–438.

[17] T. Chen, S. Yu and Y.C. Liu, Effects of pressure on propagation characteristics of methane-air edge flames within two-dimensional mixing layers: a numerical study, *Fuel* 301 (2021), 120857.

[18] V.S. Santoro, A. Liñán and A. Gomez, Propagation of edge flames in counterflow mixing layers: experiments and theory, *Proc. Combust. Inst.* 28 (2000), 2039–2046.

[19] N.I. Kim, J.I. Seo, K.C. Oh and H.D. Shin, Lift-off characteristics of triple flame with concentration gradient, *Proc. Combust. Inst.* 30 (2005), 367–374.

[20] N. Kim, J. Seo, Y. Guahk and H. Shin, The propagation of tribrachial flames in a confined channel, *Combust. Flame* 146 (2006), 168–179.

[21] M. Cha and P. Ronney, Propagation rates of nonpremixed edge flames, *Combust. Flame* 146 (2006), 312–328.

[22] H. Song, P. Wang, R.S. Boles, D. Matinyan, H. Prahanphap, J. Piotrowicz et al., Effects of mixture fraction on edge-flame propagation speeds, *Proc. Combust. Inst.* 36 (2017), 1403–1409.

[23] Z. Zhou, S.S. Applebaum and P.D. Ronney, Effect of stoichiometric mixture fraction on nonpremixed h2o2n2 edge-flames, *Proc. Combust. Inst.* 37 (2019), 1989–1996.

[24] S. Xie, Z. Lu and Z. Chen, Effects of strain rate and lewis number on forced ignition of laminar counterflow diffusion flames, *Combust. Flame* 226 (2021), 302–314.

[25] L.J. Hartley and J.W. Dold, Flame propagation in a nonuniform mixture: analysis of a propagating triple-flame, *Combust. Sci. Technol.* 80 (1991), 23–46.

[26] T. Poinsot and D. Veynante, Theoretical and Numerical Combustion, 2nd ed*Edwards*, Philadelphia, 2005.

[27] Z. Lu and M. Matalon, The speed and temperature of an edge flame stabilized in a mixing layer: dependence on fuel properties and local mixture fraction gradient, *Combust. Sci. Technol.* 192 (2020), 1274–1291.

[28] C. Pantano, Direct simulation of non-premixed flame extinction in a methane–air jet with reduced chemistry, *J. Fluid Mech.* 514 (2004), 231–270.

[29] S. Karami, E.R. Hawkes, M. Talei and J.H. Chen, Edge flame structure in a turbulent lifted flame: a direct numerical simulation study, *Combust. Flame* 169 (2016), 110–128.

[30] S. Karami, M. Talei, E.R. Hawkes and J.H. Chen, Local extinction and reignition mechanism in a turbulent lifted flame: a direct numerical simulation study, *Proc. Combust. Inst.* 36 (2017), 1685–1692.

[31] V. Nayagam, R. Balasubramaniam and P.D. Ronney, Diffusion flame-holes, *Combust. Theory Model.* 3 (1999), 727–742.

[32] V. Nayagam and F.A. Williams, Lewis-number effects on edge-flame propagation, *J. Fluid Mech.* 458 (2002), 219–228.

[33] C. Pantano and D.I. Pullin, On the dynamics of the collapse of a diffusion-flame hole, *J. Fluid Mech.* 480 (2003), 311–332.

[34] Z. Lu and S. Ghosal, Flame holes and flame disks on the surface of a diffusion flame, *J. Fluid Mech.* 513 (2004), 287–307.

[35] J. Buckmaster and T.L. Jackson, Holes in flames, flame isolas, and flame edges, *Proc. Combust. Inst.* 28 (2000), 1957–1964.

[36] Z. Chen and Y. Ju, Theoretical analysis of the evolution from ignition kernel to flame ball and planar flame, *Combust. Theory Model.* 11 (2007), 427–453.

[37] H. Zhang and Z. Chen, Spherical flame initiation and propagation with thermally sensitive intermediate kinetics, *Combust. Flame* 158 (2011), 1520–1531.

[38] F.J. Miller, J.W. Easton, A.J. Marchese and H.D. Ross, Gravitational effects on flame spread through non-homogeneous gas layers, *Proc. Combust. Inst.* 29 (2002), 2561–2567.

[39] K.K. Kuo and R. Acharya, Fundamentals of Turbulent and Multiphase Combustion, *Wiley*, Hoboken, N.J, 2012.

[40] M. Nishioka, C.K. Law and T. Takeno, A flame-controlling continuation method for generating s-curve responses with detailed chemistry, *Combust. Flame* 104 (1996), 328–342.

[41] Z. Chen, M.P. Burke, Y. Ju, On the critical flame radius and minimum ignition energy for spherical flame initiation, *Proc. Combust. Inst.* 33 (2011) 1219-1226.

[42] X. Chen, H. Bottler, A. Scholtissek, C. Hasse, Z. Chen, Effects of stretch-chemistry interaction on chemical pathways for strained and curved hydrogen/air premixed flames, *Combust. Flame* 232 (2021) 111532.

[43] X. Chen, W. Peng, P. Gillard, L. Courty, M.L. Sankhe, S. Bernard, Y. Wu, Y. Wang, Z. Chen, Effects of fuel decomposition and stratification on the forced ignition of a static flammable mixture, *Combust. Theory Model.* 25 (2021) 813-831.

[44] P. Rajamanickam, W. Coenen, A.L. Sánchez and F.A. Williams, Influences of stoichiometry on steadily propagating triple flames in counterflows, *Proc. Combust. Inst.* 37 (2019), 1971–1977.

[45] D. Yu, Z. Chen, Theoretical analysis on the transient ignition of a premixed expanding flame in a quiescent mixture, *J. Fluid Mech.* 924 (2021) A22